J. Comp. App. Res. Mech. Eng. Vol. X. No. X, pp. X-X, XXXX *DOI: 10.22061/jcarme.XXXX.XXXX.XXXX*

SRTTU

Journal of Computational and Applied Research in Mechanical Engineering

jcarme.sru.ac.ir

JCARME

ISSN: 2228-7922

Research paper

Comparative analytical study of thermal and thermo-hydraulic performance in solar air heaters with fins, baffles, porous matrix, and internal recycling

Fatemeh Karami and Majid Sabzpooshani*

Faculty of Mechanical Engineering, University of Kashan, Kashan 8731751167, Iran

Article info:

Article history:

Received: 00/00/0000

Revised: 00/00/0018

Accepted: 00/00/0000

Online: 00/00/0000

Keywords:

Solar air heater,

Porous Matrix,

Fin and baffles,

Upstream and downstream recycles,

Thermo-hydraulic efficiency.

***Corresponding author:**

spooshan@kashanu.ac.ir

Abstract

This paper presents a comparative analytical investigation of five distinct configurations of single-pass flat plate solar air heaters (SAHs), incorporating fins, baffles, porous matrix, and internal air recycling. A steady-state, one-dimensional mathematical model was developed and solved analytically to evaluate both thermal and thermo-hydraulic performance under various mass flow rates and reflux ratios. The results indicate that using a porous matrix alone results in approximately 14% lower thermal efficiency compared to configurations with fins and baffles. Placing the matrix beneath the absorber plate improved thermal efficiency by about 1.5%, but reduced thermo-hydraulic efficiency by roughly 2.5% compared to placing it above. While combining enhancement techniques does not always yield superior performance, the SAH equipped with fins and baffles alone achieved the highest thermal and thermo-hydraulic efficiencies across most conditions. Furthermore, increasing solar radiation intensity and air mass flow rate enhanced useful heat gain, although higher pressure losses caused the thermo-hydraulic efficiency to decline at elevated flow rates. Overall, this study provides valuable insights into the optimal integration of thermal enhancement methods in solar air heaters for improved energy performance.

1. Introduction

Solar energy continues gaining prominence as a clean, abundant, and sustainable alternative to fossil fuels. Among solar thermal technologies, the flat plate solar air heaters (FPSAHs) are particularly attractive due to their structural simplicity, low operational cost, and applicability in heating, drying, and ventilation processes across residential, agricultural, and industrial sectors. Despite these advantages, the broader deployment of FPSAHs is hindered by low thermal efficiency, highly attributed to weak convective heat transfer between the absorber plate and the air stream.

Over the past two decades, numerous enhancement techniques have been explored to address this limitation. Recent advanced studies have particularly focused on hybrid designs integrating multiple augmentation strategies. For

instance, Ghiami and Ghiami [1] experimentally demonstrated that adding baffles to PCM-integrated SAHs could nearly double thermal efficiency, from 14.30% to 26.78%. Ahmadkhani *et al.* [2] introduced a dual-pass system with internal air recycling and a porous matrix, achieving efficiencies up to 79%. Singh and Dhiman [3] further improved thermohydraulic performance by using a triple-channel design incorporating both porous media and internal recirculation. These modern investigations underscore the growing trend toward synergistic enhancements rather than isolated interventions.

Several configurations employing extended surfaces, such as fins and baffles, have also yielded notable improvements. Mohammadi and Sabzpooshani [4] showed analytically that combining external recycling with fins and baffles can significantly improve heat transfer, though at the cost of increased pressure drop. These findings were later validated experimentally [5], confirming the trade-offs between thermal gains and fan power requirements. Chabane *et al.* [6] and Karwa [7] also highlighted that longitudinal fins enhance thermal efficiency but require careful optimization to manage associated pumping power.

Porous media—such as metal screens, packed beds, and wire meshes—have emerged as another effective solution to enhance absorber plate-air interaction. Ahmad *et al.* [8, 9] found copper screens to be superior among various porous absorbers. Sebaii *et al.* [10] showed that gravel beds placed above the absorber enhance thermohydraulic efficiency. Velmurugan and Calaivanan [11] compared multiple porous-based SAHs and concluded that double-pass wire mesh absorbers delivered superior exergy performance.

In parallel, air recycling techniques, both internal and external, have shown promise in improving convective heat transfer by increasing air velocity. Dhiman and Singh [12] and Yeh and Ho [13] demonstrated the benefits of optimal recycle ratios on both thermal and thermohydraulic efficiency. However, as Omojaro and Aldabbagh [14] noted, higher flow rates in double-pass systems may reduce outlet temperature due to shorter residence times.

Meanwhile, surface roughness strategies, such as V-shaped and ribbed patterns, have proven to be effective in inducing turbulence. Momin *et al.* [15], Saini and Singal [16], and Hans *et al.* [17] developed key correlations between rib geometry and heat transfer rates. Ravi and Saini [18] showed that multi-V ribs could enhance thermal performance by up to 4.5 times, albeit with a significant rise in friction factor. Singh [19] proposed a porous spiral-wavy duct, emphasizing the influence of porosity and interface resistance on SAH performance.

Despite significant advancements in enhancing the performance of solar air heaters (SAHs) through individual strategies such as surface roughness, fins, baffles, porous matrices, and air recycling, most prior studies have investigated these techniques in isolation or limited combinations. These fragmented approaches often lack a unified analytical framework that enables a comprehensive comparison of various enhancement methods under consistent boundary conditions. Additionally, critical aspects such as the positional placement of porous matrices—particularly their effect when located above versus below the absorber plate—have not been adequately addressed in the literature.

2. Objective

To bridge the gaps mentioned, the present study introduces a novel and unified analytical investigation of five distinct single-pass solar air heater configurations that integrate various combinations of internal air recycling, absorber-plate-mounted fins and baffles, and porous matrices placed in different locations. A one-dimensional, steady-state, approximate analytical model is developed and validated against existing experimental results to assess both thermal and thermohydraulic performance under varying operating conditions, including mass flow rates, recycle ratios, and solar radiation intensities. The main contributions of this study, distinguishing it from previous works, are:

(1) Development of a comprehensive and unified analytical model that simultaneously incorporates internal air recycling, absorber-plate-mounted fins and baffles, and porous matrix configurations—elements that have rarely been combined in a single framework;
(2) Novel investigation of the effects of porous matrix placement above versus below the absorber plate on both thermal performance and pressure drop, a topic scarcely addressed or compared in existing literature;
(3) Systematic parametric analysis over a wide range of operating conditions (mass flow rate, recycle ratio, solar intensity) providing actionable insights and practical design guidelines that enable optimized trade-offs between enhanced heat transfer and pressure losses;
(4) Validation of the model against existing data to ensure accuracy and applicability, enhancing the reliability of design recommendations for advanced solar air heater systems.
This work advances the field by moving beyond isolated or limited enhancement studies and presents, for the first time, a comprehensive comparative investigation of a double-pass solar air heater, combining fins, baffles, and a porous matrix within an internal heat recovery system. This study provides detailed insights into the thermal, hydraulic, and thermo-hydraulic behavior across various configurations under different mass flow rates and reflux ratios, offering a holistic approach that can guide more effective and integrated solar air heater designs.

3. Methods

3.1. Theoretical study

In this study, an approximate analytical investigation was conducted to evaluate the possibility of improving the performance of the considered solar air heater with internal recycling by using fins, baffles, and a porous matrix in various configurations.

3.2. Description of five air heaters types

In the design and classification of air heaters, five distinct models have been developed. It is noteworthy to mention that in these air heaters, a specific set of materials has been utilized, including two glass covers, a steel plate placed beneath the second glass cover functions as the absorber, while a polished stainless-steel plate positioned below it serves as the back plate, with a wooden layer providing insulation.
The first model features a central air channel where air passes for heating, while the lower channel serves as the recycling path (Fig. 1(a)).
The second model incorporates a matrix in the central air channel, which enhances heat transfer efficiency as the air flows through it. The lower channel remains the recycling path (Fig. 1(b)).
In the third model, the primary air passage for heating is through the lower channel, where a matrix is placed beneath the absorber plate, while the central channel is used for air recycling (Fig. 1(c)).
The fourth model introduces fins and baffles into the central air channel to improve heat transfer. The matrix is located in the lower channel, which serves as the recycling path (Fig. 1(d)).
The fifth model includes fins and baffles in the central air channel but does not have a matrix. The lower channel is solely dedicated to air recycling (Fig. 1(e)).

3.3. Analytical investigations

In the formulation of mathematical models for single-pass solar air heaters, the following assumptions have been taken into account:

1. Steady State Operation: The system is assumed to operate under steady-state conditions.
2. One-Dimensional Air Flow: Air flow within the system is treated as one-dimensional, with the primary direction along the X axis.
3. Negligible Shadowing: Effects of walls casting shadows on the absorber plate are considered negligible.
4. Sky Representation: A black body with a corresponding temperature is used to represent the sky.
5. Mean Temperature Thermo-Physical Properties: The mean temperature is used as the basis for calculating the thermo-physical properties of the airflow. (The thermo-physical properties of air are evaluated at the mean temperature between the inlet and outlet.

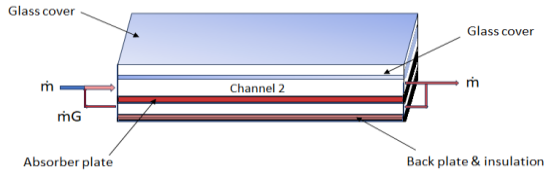

(a) Conventional SAH (Type 1)

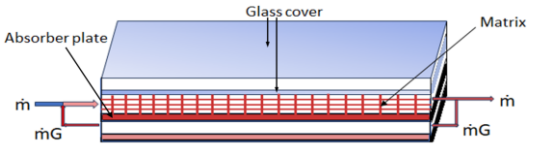

(b) SAH with matrix above absorber plate (Type 2)

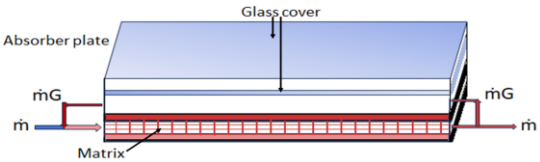

(c) SAH with matrix below absorber plate (Type 3)

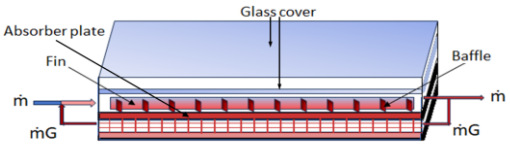

(d) SAH with fins and baffles and matrix in recycle duct (Type 4)

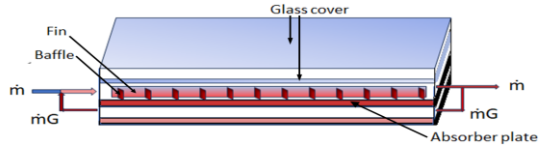

(e) SAH with fins and baffles only (Type 5)

Fig. 1. Physical models of the five investigated solar air heater configurations: (a) Conventional SAH (Type 1), (b) SAH with matrix above absorber plate (Type 2), (c) SAH with matrix below absorber plate (Type 3), (d) SAH with fins and baffles and matrix in recycle duct (Type 4), (e) SAH with fins and baffles only (Type 5).

This assumption is generally valid for laminar and early transitional regimes (Re < 4000) [20]. While this simplification introduces minor deviations in transitional flow conditions, it remains widely used in semi-analytical and engineering analyses due to its computational efficiency and acceptable accuracy [21].)

6. Absence of Temperature Gradients: Temperature gradients within the cover, back plate, and absorber plate are assumed to be nonexistent.
7. Negligible Heat Losses: Heat losses from the edges and at the inlet of the recycling channel are deemed insignificant.

3.3.1. The energy balance equations

The energy balance equations for the components of five types of solar air heaters are examined separately in Table 1.
The thermophysical properties of materials used in the construction of the five systems, such as absorptivity, transmissivity, and emissivity, are provided in Table 2, as they are essential inputs for accurate thermal modeling.
The structural and design specifications of the porous matrix used in the packed bed solar air heater configurations are summarized in Table 3. These parameters significantly influence heat transfer enhancement and pressure drop within the system.
Table 4 provides the geometrical dimensions and arrangement details of the fins and baffles incorporated in the enhanced solar air heater model. These components are designed to increase the heat transfer surface area and promote turbulent mixing, thereby improving overall thermal performance.
In Fig. 2, as an example, the energy balance equation for a differential control volume considered in the airflow passing through channel 2 in solar air heater Type 1 is analyzed.

$$\phi\dot{m}(1+G)C_p\left(T_{f2}\big|_{x+dx}-T_{f2}\big|_x\right)= h_{c,gl-f2}(T_{gl}-T_{f2})(wdx) +h_{c,p-f2}(T_p-T_{f2})(wdx)$$

$$\xrightarrow{yields}$$

$$\dot{m}(1+G)C_p\left(\frac{dT_{f2}(x)}{dx}\right)=h_{c,gl-f2}(T_{gl}-T_{f2})+h_{c,p-f2}(T_p-T_{f2}) \quad (1)$$

The value of ϕ presented in Table 1 is defined as follows [5]:

$$\phi=1+\frac{A_{fin}}{A_p-A_{finb}}\eta_{fin}+\frac{A_{baff}}{A_p-A_{finb}}\eta_{baff} \quad (2)$$

η_{fin} is the fin efficiency and can be obtained as [5]:

$$\eta_{fin} = \frac{\tanh(Mh_{fin})}{Mh_{fin}} \quad (3)$$

$$M = \left(\frac{2h_{c,p-f}(L + t_{fin})}{kLt_{fin}}\right)^{\frac{1}{2}} \quad (4)$$

η_{baff} is the baffle efficiency which may be obtained as [5]:

$$\eta_{baff} = 15.583\left(\frac{w_{baff}}{D_h}\right)^{0.0518}\left(\frac{L}{L_{baff}}\right)^{-0.2247} \quad (5)$$

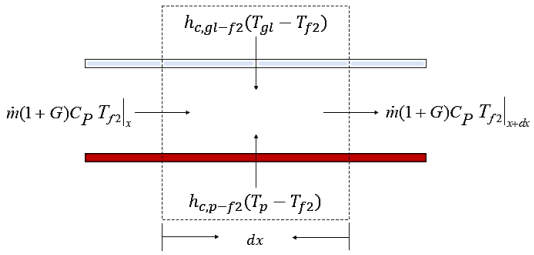

Fig. 2. A differential control volume in the airflow passing through channel 2 in solar air heater Type 1.

Table 1. Energy balance equations applied to each component in the five solar air heater configurations studied.

The energy balance equation	Component	Type
$h_w(T_{gu} - T_a) + h_{r,gu-s}(T_{gu} - T_s) + h_{r,gu-gl}(T_{gu} - T_{gl}) = I\alpha_{gu}$	Upper glass cover	All Types
$h_{r,gl-gu}(T_{gl} - T_{gu}) + h_{r,gl-p}(T_{gl} - T_P) + h_{c,gl-f2}(T_{gl} - T_{f2,avg}) = I\tau_{gu}\alpha_{gl}$	Lower glass cover	Types 1,3,4,5
$h_{r,gl-gu}(T_{gl} - T_{gu}) + h_{r,gl-m}(T_{gl} - T_m) + h_{c,gl-f2}(T_{gl} - T_{f2,avg}) = I\tau_{gu}\alpha_{gl}$	Lower glass cover	Type 2
$h_{r,p-gl}(T_p - T_{gl}) + h_{c,p-f2}(T_p - T_{f2,avg}) + h_{r,p-b}(T_p - T_b) + h_{c,p-f3}(T_p - T_{f3,avg}) = I\tau_{gu}\tau_{gl}\alpha_p$	Absorber plate	Type 1
$h_{r,p-m}(T_p - T_m) + h_{c,p-f2}(T_p - T_{f2,avg}) + h_{r,p-b}(T_p - T_b) + h_{c,p-f3}(T_p - T_{f3,avg}) = 0$	Absorber plate	Type 2
$h_{r,p-gl}(T_p - T_{gl}) + h_{c,p-f2}(T_p - T_{f2,avg}) + h_{r,p-m}(T_p - T_m) + h_{c,p-f3}(T_p - T_{f3,avg}) = I\tau_{gu}\tau_{gl}\alpha_p$	Absorber plate	Type 3
$h_{r,p-gl}(T_p - T_{gl}) + \phi h_{c,p-f2}(T_p - T_{f2,avg}) + h_{r,p-m}(T_p - T_m) + h_{c,p-f3}(T_p - T_{f3,avg}) = I\tau_{gu}\tau_{gl}\alpha_p$	Absorber plate	Type 4
$h_{r,p-gl}(T_p - T_{gl}) + \phi h_{c,p-f2}(T_p - T_{f2,avg}) + h_{c,p-f3}(T_p - T_{f3,avg}) = I\tau_{gu}\tau_{gl}\alpha_p$	Absorber plate	Type 5
$h_{r,m-p}A_p(T_m - T_p) + h_{c,m-f2}A_m(T_m - T_{f2,avg}) + h_{r,m-gl}A_{gl}(T_m - T_{gl}) = A_m I\tau_{gu}\tau_{gl}\alpha_m$	Matrix	Type 2
$h_{r,m-p}A_p(T_m - T_p) + h_{c,m-f3}A_m(T_m - T_{f3,avg}) + h_{r,m-b}A_b(T_m - T_b) = 0$	Matrix	Types 3, 4
$h_{r,b-p}(T_b - T_p) + h_{c,b-f3}(T_b - T_{f3,avg}) + U_b(T_b - T_a) = 0$	Back plate	Types 1, 2, 5
$h_{r,b-m}(T_b - T_m) + h_{c,b-f3}(T_b - T_{f3,avg}) + U_b(T_b - T_a) = 0$	Back plate	Types 3, 4
$\frac{\dot{m}(1+G)C_P}{w}\frac{dT_{f2}(x)}{dx} = h_{c,gl-f2}(T_{gl} - T_{f2}(x)) + h_{c,p-f2}(T_p - T_{f2}(x))$	Air flow (channel 2)	Type 1
$\frac{\dot{m}(1+G)C_P}{w}\frac{dT_{f2}(x)}{dx} = h_{c,gl-f2}(T_{gl} - T_{f2}(x)) + h_{c,m-f2}(T_m - T_{f2}(x)) + h_{c,p-f2}(T_p - T_{f2}(x))$	Air flow (channel 2)	Type 2
$\frac{\dot{m}GC_P}{w}\frac{dT_{f2}(x)}{dx} = h_{c,gl-f2}(T_{gl} - T_{f2}(x)) + h_{c,p-f2}(T_p - T_{f2}(x))$	Air flow (channel 2)	Type 3
$\frac{\dot{m}(1+G)C_P}{w}\frac{dT_{f2}(x)}{dx} = h_{c,gl-f2}(T_{gl} - T_{f2}(x)) + \phi h_{c,p-f2}(T_p - T_{f2}(x))$	Air flow (channel 2)	Types 4, 5
$\frac{\dot{m}GC_P}{w}\frac{dT_{f3}(x)}{dx} = h_{c,b-f3}(T_b - T_{f3}(x)) + h_{c,p-f3}(T_p - T_{f3}(x))$	Air flow (channel 3)	Types 1, 2, 5
$\frac{\dot{m}(1+G)C_P}{w}\frac{dT_{f3}(x)}{dx} = h_{c,b-f3}\left(T_b - T_{f3}(x)\right) + h_{c,m-f3}\left(T_m - T_{f3}(x)\right) + h_{c,p-f3}(T_p - T_{f3}(x))$	Air flow (channel 3)	Type 3
$\frac{\dot{m}GC_P}{w}\frac{dT_{f3}(x)}{dx} = h_{c,b-f3}\left(T_b - T_{f3}(x)\right) + h_{c,m-f3}\left(T_m - T_{f3}(x)\right) + h_{c,p-f3}(T_p - T_{f3}(x))$	Air flow (channel 3)	Type 4

Table 2. Thermophysical properties of materials used in the construction of the five solar air heater systems.

Components	Width (m)	Length (m)	Depth (m)	Thickness (m)	Absorptivity (α)	Transmissivity (τ)	Emissivity (ε)
Transparent cover	0.45	2.2	------	0.003	0.05	0.95	0.92
Absorber plate	0.45	2.2	------	0.003	0.95	------	0.9
Matrix	0.45	2.2	0.06	------	0.95	------	0.9
Back plate	0.45	2.2	------	0.003	------	------	0.94
Insulation	0.45	2.2	------	0.05	------	------	------
Channels 1, 2, and 3	0.45	2.2	0.06	------	------	------	------

Table 3. Structural characteristics and design parameters of the porous matrix used in the packed bed solar air heater configurations.

Type of matrix	d_w (mm)	p_t (mm)	n	P
M3	0.4	1	12	0.95

Table 4. Geometrical dimensions and arrangement details of fins and baffles in the enhanced solar air heater model.

Number of fins (N)	Width of baffle (w_{baff})	Height of fins (H_{fin})	Distance between baffles (L_{baff})	Thickness of fins (t_{fin})
3	0.07 m	0.06 m	0.4 m	0.001 m

3.3.2. Heat transfer coefficients

Since all sheets of the SPFSAH are parallel, flat, and near to one another, their shape factors relative to each other are assumed to be 1. Consequently, the radiative heat transfer coefficients are determined accordingly [12]:

$$h_{r,gu-s} = \sigma\varepsilon_{gu}({T_{gu}}^2 + {T_s}^2)(T_{gu} + T_s) \quad (6)$$

$$h_{r,gu-gl} = \frac{\sigma({T_{gu}}^2 + {T_{gl}}^2)(T_{gu} + T_{gl})}{\frac{1}{\varepsilon_{gu}} + \frac{1}{\varepsilon_{gl}} - 1} \quad (7)$$

$$h_{r,gl-m} = \frac{\sigma({T_{gl}}^2 + {T_m}^2)(T_{gl} + T_m)}{\frac{1}{\varepsilon_{gl}} + \frac{1}{\varepsilon_m} - 1} \quad (8)$$

$$h_{r,m-p} = \frac{\sigma({T_m}^2 + {T_p}^2)(T_m + T_p)}{\frac{1}{\varepsilon_m} + \frac{1}{\varepsilon_p} - 1} \quad (9)$$

$$h_{r,p-b} = \frac{\sigma({T_p}^2 + {T_b}^2)(T_p + T_b)}{\frac{1}{\varepsilon_p} + \frac{1}{\varepsilon_b} - 1} \quad (10)$$

where ε is the emissivity of the surface whose values are listed in Table 2, the temperature (T) is in Kelvin, and the Boltzmann constant is σ, which is considered as 5.67×10^{-8} W/m^{2}K^4. T_S is the equivalent sky temperature, which is measured as [2]:

$$T_s = 0.0552{T_a}^{1.5} \quad (11)$$

The convection heat transfer coefficient, h_w, associated with the wind-induced flow over the upper glass cover is derived using the following correlation [2]:

$$h_w = 5.7 + 3.8V \quad (12)$$

where V is the wind velocity.

- When there is no matrix in the channel:

The Nusselt number for air flowing through the channel for laminar flow can be calculated using the following empirical correlation proposed by Sopian *et al.* [22]:

$$Nu = \frac{h_c D_h}{k_f} = 5.4 + \frac{0.0019[Re.Pr\left(\frac{D_h}{L}\right)]^{1.71}}{1 + 0.00563[Re.Pr(\frac{D_h}{L})^{1.17}]} \quad (13)$$

for Re<2300

and for transitional flow in the channel, the Nusselt number is calculated by [22]:

$$Nu = \frac{h_c D_h}{k_f} = 0.116\left(Re^{\frac{2}{3}} - 125\right)Pr^{\frac{1}{3}} \times \left(1 + \left(\frac{D_h}{L}\right)^{\frac{2}{3}}\right)\left(\frac{\mu}{\mu_w}\right)^{0.14} \quad (14)$$

for 2300<Re<6000

where μ_W is the viscosity at the wall temperature. For the fully developed turbulent flow in the channel, the Nusselt number is estimated by [22]:

$$Nu = \frac{h_c D_h}{k_f} = 0.118 Re^{0.8} Pr^{0.4}$$

for Re>6000 (15)

where k_f is the conductivity of air.
These equations are empirical correlations specifically developed by Sopian *et al.* [22] for solar air heater channels. While Eq. (15) resembles the well-known Dittus–Boelter correlation, it differs in the empirical coefficient (0.118 instead of 0.023), indicating experimental calibration for solar collector applications. These correlations are distinct from the Gnielinski equation and are not derived from it.
The hydraulic diameter of the channel when there is no fin and baffle is defined as follows:

$$D_h = \frac{4A_f}{y} = \frac{4wd}{2(w+d)} = \frac{2wd}{w+d} \quad (16)$$

and when there are fins and baffles the D_h and Reynolds number are calculated from the following relations [5]:

$$D_h = \frac{2(wd - NH_{fin}t_{fin})}{(w+d) + N(H_{fin} + t_{fin})} \quad (17)$$

$$Re = \frac{\rho v D_h}{\mu_f} = \frac{2\dot{m}}{\mu_f\left((w+d) + N\left(H_{fin} + t_{fin}\right)\right)} \quad (18)$$

- For matrix in the channel:

The convective heat transfer coefficient between channel wall and air flowing through the channel with matrix can be estimated by the following relationship:

$$h_c = \frac{Nu_m k_f}{P D_h} \quad (19)$$

where D_h is calculated from equation 16, P and Nu_m are the porosity and Nusselt number of porous medium, which are calculated from the following relations [23]:

$$P = \frac{{p_t}^2 d - [\frac{\pi}{2}(d_w)^2 p_t]n}{{p_t}^2 d} \quad (20)$$

$$Nu_m = 0.2 {Re_m}^{0.8} Pr^{\frac{1}{3}} \quad (21)$$

in which Re_m is calculated from [23]:

$$Re_m = \frac{4 r_h G_0}{\mu} \quad (22)$$

where r_h and G_0 are the hydraulic radius and mass velocity, which are calculated from the following relations:

$$r_h = \frac{P d_w}{4(1-P)} \quad (23)$$

$$G_0 = \frac{\dot{m}}{A_f P} \quad (24)$$

The heat transfer coefficient due to convection between the air passing through the flow channels and the matrix is obtained from [2]:

$$h_{c,m-f} = St_m G_0 C_p \quad (25)$$

where St_m is calculated from:

$$St_m = J_H Pr^{-\frac{2}{3}} \quad (26)$$

Also, the Colburn J-factor is given by [2]:

$$J_H = 0.64\left(\frac{1}{nP}\left(\frac{p_t}{d_w}\right)\right)^{2.104} {Re_m}^{-0.55} \quad (27)$$

3.3.3. Solution process and boundary conditions

The linear differential equations for air flow in the channel have been solved analytically using the following boundary conditions associated with the SPFSAH of Types 1, 2, 4, and 5:

$$T_{f2@x=0} = \frac{G T_{f3@x=L} + T_a}{(1+G)} \quad (28)$$

$$T_{f3@x=0} = T_{f2@x=L} \quad (29)$$

For SPFSAH Type 3, the boundary conditions are as follows:

$$T_{f2@x=0} = \frac{GT_{f1@x=L} + T_a}{(1+G)} \quad (30)$$

$$T_{f3@x=0} = T_a \quad (31)$$

The average temperature in channels 2 and 3 is defined using the mean value theorem:

$$T_{f,avg} = \frac{1}{L}\int_0^L T_f(x)dx \quad (32)$$

The energy gained by the air as it flows through the channels, known as the useful heat transfer in the SPFSAH, is analyzed for configurations 1, 2, 4, and 5, and is given by:

$$Q_u = \dot{m}(1+G)C_p\left(T_{f2@x=L} - T_{f2@x=0}\right) + \dot{m}GC_p(T_{f3@x=L} - T_{f3@x=0}) \quad (33)$$

For Type 3, this parameter is estimated by:

$$Q_u = \dot{m}GC_p\left(T_{f2@x=L} - T_{f2@x=0}\right) + \dot{m}(1+G)C_p(T_{f3@x=L} - T_{f3@x=0}) \quad (34)$$

Thus, the thermal efficiency η_{th} of the heater can be calculated by:

$$\eta_{th} = \frac{Q_u}{IA_{co}} \quad (35)$$

However, due to the increase in pressure drop and pump work caused by fins and baffles attached to the absorber plate and matrix configurations, the thermo-hydraulic efficiency is a more reliable index for analyzing the energy performance of the air heater. The thermo-hydraulic efficiency is defined as [2]:

$$\eta_{thy} = \frac{Q_u - P_{fan}}{IA_{co}} \quad (36)$$

where P_{fan} is defined as the fan power [2]:

$$P_{fan} = \frac{P_{flow}}{\eta_f \eta_m} \quad (37)$$

in which and η_m and η_f are considered to be 0.9 and 0.7, respectively [24]. Furthermore, P_{flow} is the air pumping power calculated for the SPFSAHs of Type 1 as:

$$P_{flow} = \frac{\dot{m}(1+G)(\Delta P_{s.d}) + \dot{m}G(\Delta P_{s.d})}{\rho} \quad (38)$$

and for the SPFSAHs of Typed 2 and 3:

$$P_{flow} = \frac{\dot{m}(1+G)\left(\Delta P_{p.d}\right) + \dot{m}G(\Delta P_{s.d})}{\rho} \quad (39)$$

and for the SPFSAHs of Type 4:

$$P_{flow} = \frac{\dot{m}(1+G)\left(\Delta P_{f.b}\right) + \dot{m}G\left(\Delta P_{p.d}\right)}{\rho} \quad (40)$$

and for Type 5:

$$P_{flow} = \frac{\dot{m}(1+G)\left(\Delta P_{f.b}\right) + \dot{m}G(\Delta P_{s.d})}{\rho} \quad (41)$$

in which $\Delta P_{f,b}$ is the pressure drop in the channel of the air heater with fins and baffles attached to the absorber plate, $\Delta P_{s,d}$ and $\Delta P_{p,d}$ are the pressure losses in the smooth duct and packed duct, separately gained from [5, 2, 24]:

$$\Delta P_{f,b} = (1.465 \times 10^{-5}) Re^{1.94} \left(\frac{W_{baff}}{D_h}\right)^{2.6} \left(\frac{L}{L_{baff}}\right)^{1.2} \quad (42)$$

$$\Delta P_{p,d} = f_m \left(\frac{\rho\left(v_f\right)^2}{2}\right)\left(\frac{L}{r_h}\right) \quad (43)$$

$$\Delta P_{s,d} = \frac{2\rho f (u_j)^2 L}{D_h} \qquad j=1,2,3 \quad (44)$$

The friction factors of the smooth and packed bed channels are represented by f and f_m, respectively. The subscript j in u_j^2 indicates the channel number through which the air flows. The parameters f and f_m are defined as follows [24]:

$$f = 0.059 Re^{-0.2} \quad (45)$$

$$f_m = 2.484 \left(\left(\frac{1}{nP}\right)\left(\frac{p_t}{d_w}\right)\right)^{0.699} {Re_m}^{-0.44} \quad (46)$$

As an example, to determine the temperatures of the various components of the SPFSAH Type 4, using the five equations provided for its components in Table 1, along with the equations for $T_{f2,avg}$, $T_{f3,avg}$, $T_{f2@x=L}$ and $T_{f3@x=L}$ derived from integrating the energy balance equations for the flow through the channels, which are also provided in Table 1, a system of nine equations with nine unknowns is obtained. In this system, the coefficients of radiative heat transfer are influenced by the component temperatures, whose values are unknown. As a result, an iterative approach is employed, starting with initial temperature estimates to solve the system. All types of SPFSAHs are solved similarly. The solution procedure, implemented in MATLAB, involves the following steps:

1. Enter the parameters that are constant G, $\dot{m}$, n, w, I, L, A_p, d_2, d_3, A_{gl}, A_b, A_m, d_w, P_t, T_a, α_{gl}, α_{gu}, K_{f2}, $K_{f3,}$ $\alpha_{p,}$ α_m, N, $w_{baff,}$ H_{baff}, L_{baff}, ε_{gl}, ε_{gu}, ε_m, $\varepsilon_{p,}$ ε_b,H_{fin}, t_{fin}, τ_{gl}, τ_{gu}, C_p, U_b, σ, V into the software.

2. Calculate Dh_3, Dh_2, Re_2, A_{f3}, J_H, r_h, G_0, Nu_m, Re_m, St_m, T_s, h_w, Nu_2, $h_{c,b\text{-}f3}$, $h_{c,m\text{-}f3}$, $h_{c,gl\text{-}f2}$, $h_{c,p\text{-}f3}$, $h_{c,p\text{-}f2}$, A_{baff}, A_{fin}, A_{finb}, η_{baff}, η_{fin}, M, ϕ, v_{f3}, f_m, ΔP_2, ΔP_3, P_{flow}, $P_{fan.}$

3. Initially assign the same value as T_a to T_{gu}, T_{gl}, T_p, T_b, T_m.

4. Based on the assumed temperatures, acquire $h_{r,gu\text{-}s}$, $h_{r,gu\text{-}gl}$, $h_{r,p\text{-}m}$, $h_{r,m\text{-}b}$, and $h_{r,p\text{-}gl}$.

5. Specify new values for T_{gl}, T_{gu}, T_p, T_b, and T_m by solving the 9×9 system of equations, using these values as the starting point for step 3.

6. Perform steps 4 and 5 again until the obtained values converge to the final calculated values.

7 .After convergence, introduce $T_{f2,avg}$, $T_{f3,avg}$, $T_{f2@x=L}$, $T_{f3@x=L}$, and estimate useful heat gain, thermal efficiency, and thermo-hydraulic efficiency.

3.4. Validating the present results

The Type 2 design examined in this research is the same as Type C of the article [2], and for the purpose of validation, the results of these two studies have been compared according to Table 5 and Fig. 3. As it is known, the relative error is less than one percent and the thermal efficiency are close to each other in the investigated conditions.

4. Results and discussion

The results of this study have been validated against the data reported by Ahmadkhani *et al.* [2]. The close agreement between the findings indicates the accuracy of the proposed model at a given mass flow rate.

An increase in the reflux ratio often leads to improvements in both useful heat gain and thermal efficiency across the various solar air heaters examined in this study. With the increase in the reflux ratio (G), a larger portion of the air mass is directed into the recycling channel, leading to an enhancement in the useful heat gain within this region [2,13].

Nevertheless, due to the lack of thermal insulation and the resultant heat exchange between the recycling channel and the main air channel, the thermal performance of the main channel is concurrently influenced. This thermal interaction and its consequences are clearly depicted in Fig. 4.

Solar air heaters of Type 5 exhibit higher useful heat and thermal efficiency compared to the others. Moreover, at flow rates of 0.01 and 0.015 kg/s (in this study), the use of a matrix in the main air passage, combined with an appropriate reflux ratio, enhances both useful heat gain and thermal efficiency. This observation aligns well with the findings of Singh and Dhiman [3], who demonstrated that packed bed configurations operating under recirculating flow conditions significantly enhance thermal performance.

Furthermore, at a mass flow rate of 0.025 kg/s and a reflux ratio less than 0.7, this trend continues.

This improvement stems from the matrix's dual role in intensifying airflow turbulence and enhancing energy exchange mechanisms within the flow domain, both of which contribute to a higher convective heat transfer coefficient.

Consequently, the air temperature in the matrix-equipped duct is higher compared to channels without the matrix. Nevertheless, attention must be paid to the increased energy demand on the fan due to the substantial pressure drop, a trade-off also reported by Singh [19].

Table 5. Validation of the present numerical model through comparison with results from Ahmadkhani *et al.* [2].

L (m)	The temperature of the air exiting from channel 2 of the Type 2 air heater in the present study (K)	The amount of difference between the results of the present study and the article [22] divided by the outlet temperature
1.8	349.1556	0.0075
1.9	350.5868	0.0068
2	351.5907	0.0046
2.1	352.574	0.0037
2.2	353.5371	0.0014

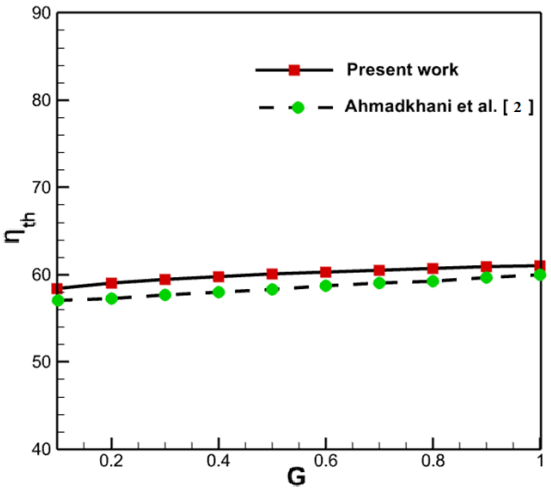

Fig. 3. Comparison of the thermal efficiencies of the Type 2 air heater in the present study with the research conducted by Ahmadkhani *et al.* [2].

At a reflux ratio of 0.1 and across all mass flow rates considered, the difference in useful heat and thermal efficiency between Type 2 and Type 3 air heaters are minimal. This indicates that, in this range, the positioning of the matrix, whether beneath or above the absorber plate, has a small impact. However, as the reflux ratio increases, this difference becomes more significant.

It is more advantageous to place the matrix beneath the absorber plate in the main air passage (Type 3), as it results in higher thermal efficiency and useful heat. This is because, in Type 3 air heaters, the absorber plate directly receives solar radiation and heats efficiently.

While the matrix in the third channel promotes turbulent mixing and offers an extended interface for energy exchange. In contrast, in Type 2 air heaters, the matrix itself functions as the absorber, and the absorber plate is shielded from solar radiation.

Fig. 5 indicates that with an increase in mass flow rate at different return coefficients, the useful heat and consequently the thermal efficiency increase in the examined types of air heaters [1,3]. The useful heat gain and thermal efficiency of Type 5 solar air heaters are significantly higher than those of other designs.

At a mass flow rate of 0.015 kg/s and a reflux ratio of 0.5, the thermal efficiency of the Type 5 air heater is approximately 13.5% greater than that of the Type 3. This demonstrates the more pronounced positive effect of using fins and baffles compared to a matrix.

Type 5 also outperforms Type 4 in both useful heat and thermal efficiency. At G=1 and m=0.01 kg/s, Type 5's thermal efficiency is 4.4% higher than Type 4. This suggests that when fins and baffles are utilized in the main flow path, adding a matrix in the return path not only fails to enhance efficiency but actually reduces it.

Although the matrix facilitates greater thermal absorption in the secondary channel, it simultaneously diverts part of the thermal energy from the absorber plate, despite its enhancement through fins and baffles. This reduces the absorber plate's temperature and decreases heat transfer to the air in the main channel. The reduction in useful heat in the second channel is greater than the increase in the third channel, resulting in an overall decrease in total useful heat and thermal efficiency.

At reflux ratios of 0.5 and 1, employing a matrix under the absorber plate (Type 3) yields higher useful heat and thermal efficiency compared to Type 2 air heaters. At a reflux ratio of 1 and a mass flow rate higher than 0.017 kg/s, the thermal efficiency and useful heat of Type 1 air heaters are higher than those of Type 2. As the mass flow rate increases, this difference becomes more significant. Therefore, within this range, a solar air heater without a matrix can replace Type 2 air heaters, leading to savings in the costs associated with matrix preparation and increased fan power consumption [2].

As solar radiation intensity increases, the useful heat absorbed also rises since the solar heater captures more energy, as evidenced by the data presented in Table 6.

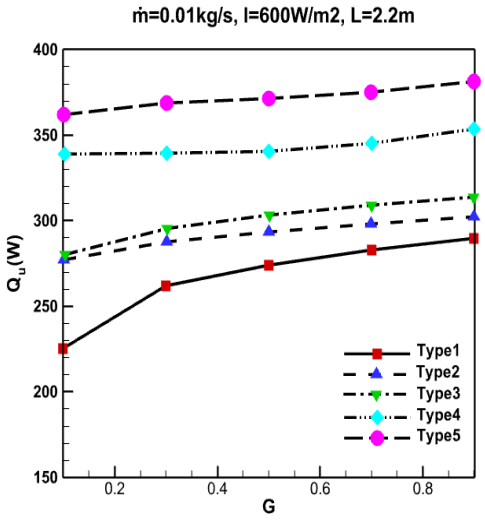

(a) ṁ=0.01 kg/s

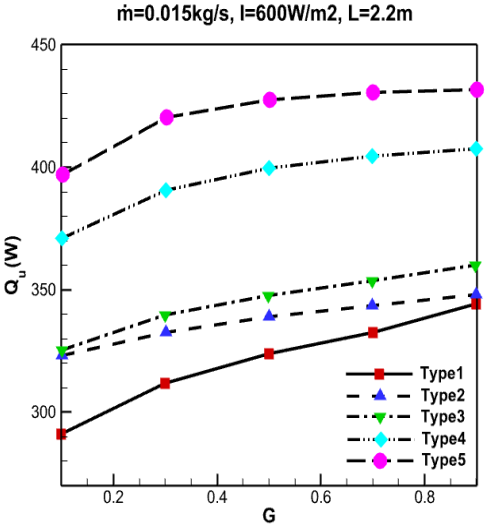

(b) ṁ=0.015 kg/s

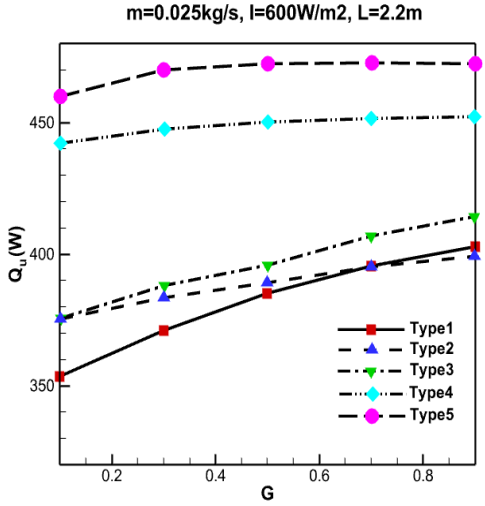

(c) ṁ=0.025 kg/s

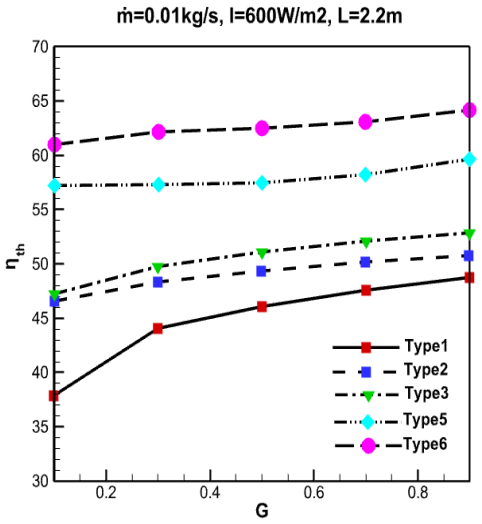

(d) ṁ=0.01 kg/s

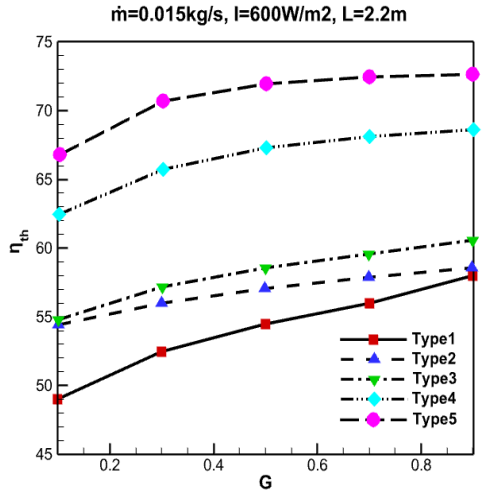

(e) ṁ=0.015 kg/s

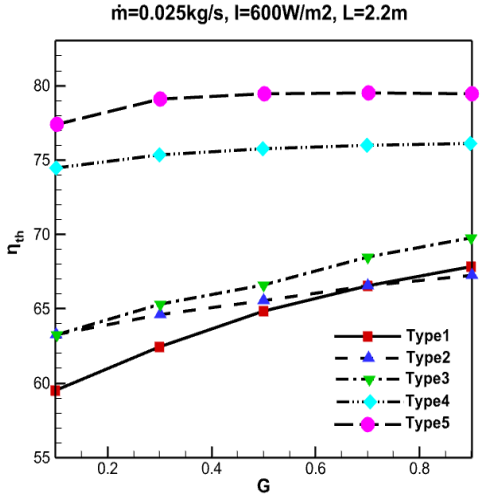

(f) ṁ=0.025kg/s

Fig. 4. Variation of useful heat gain and thermal efficiency with reflux ratio (G) under constant solar irradiance (I = 600 W/m²) for different mass flow rates: (a) Q_u for ṁ=0.01 kg/s, (b) Q_u for ṁ=0.015 kg/s, (c) Q_u for ṁ=0.025 kg/s, (d) η_{th} for ṁ=0.01 kg/s, (e) η_{th} for ṁ=0.015 kg/s, (f) η_{th} for ṁ=0.025 kg/s.

However, this does not necessarily imply that the thermal efficiency will increase as well. According to Equation 35, used to calculate thermal efficiency, both Q_u and I increase, and the relative increase in these two variables will ultimately determine whether the thermal efficiency improves or decreases [20].

Fig. 6 shows how thermal and thermo-hydraulic efficiencies change with the reflux ratio when the mass flow rate is 0.01 kg/s. It demonstrates that in the Type 1 air heater, thermal and thermo-hydraulic efficiencies are approximately equal due to the smooth air passage channel and low pressure drop [2]. However, in other types of air heaters studied, thermo-hydraulic efficiency is reduced compared to thermal efficiency because of the pressure drop resulting from the presence of matrices, fins, or baffles [4,19].

At 0.01 kg/s mass flow rate, in Types 1, 2, and 3 air heaters, with increasing reflux ratio, both thermal and thermo-hydraulic efficiencies increase [13]. In Type 4, where fins, baffles, and matrices are used, thermo-hydraulic efficiency initially decreases as the reflux ratio (G) increases to less than 0.5, but it subsequently increases when G exceeds 0.5. It should be noted that in Types 4 and 5 air heaters, this increasing trend continues and halts at reflux ratios greater than 0.9. The change in the trend of the graphs is due to the use of different heat transfer coefficients for laminar and turbulent regimes [4].

Fig. 7 compares the thermo-hydraulic efficiency of different air heaters at a mass flow rate of 0.01 kg/s and various return ratios. As shown in the figure, the thermo-hydraulic efficiency of Type 5 is higher than that of other types, indicating that using fins and baffles in the air heater structure is more effective than using matrices. Additionally, the combination of both not only fails to improve efficiency but also decreases it.

At a 0.01 kg/s mass flow rate of and different return ratios, the thermo-hydraulic efficiency of Type 3 is higher than that of Type 2, suggesting that at this mass flow rate, a matrix under the absorber plate is more effective than one on top of the absorber plate. The thermo-hydraulic efficiency of Type 1 air heaters is the lowest.

Fig. 8 compares the thermo-hydraulic efficiency of air heaters at different mass flow rates and a constant return ratio. As seen from the graphs, the thermo-hydraulic efficiency of Type 5 is the highest across all examined mass flow rates, and at return ratios G=0.1 and G=0.5. At all examined return ratios, when the mass flow rate exceeds approximately 0.015 kg/s, the thermo-hydraulic efficiency of Type 2 is higher than Type 3, with the difference increasing as the mass flow rate increases.

Considering that part of the present study focuses on investigating the effects of the placement of the porous matrix in solar air heaters, it is essential to compare the obtained results with previous related studies in order to clarify the research context and highlight the key differences. One notable study by Sebaii et al. [10] examined similar configurations involving porous matrices, providing valuable insights into the thermal and thermo-hydraulic performance of double glass, double pass solar air heaters with packed beds. Although at first glance some results may appear contradictory to the present work, it is crucial to recognize that the geometric arrangements and airflow paths differ significantly between the two studies, which fundamentally impacts the outcomes.

In the study conducted by Sebaii et al. [10], the main airflow path was considered above the absorber plate in both configurations examined.The only difference between the two cases lay in the placement of the porous matrix: in one scenario, it was located above the absorber in the main flow path, while in the other, it was placed beneath the absorber in the recycle path. In contrast, in Configuration 3 of the present study, the porous matrix is placed beneath the absorber plate, and the primary airflow path also passes below the absorber plate; thus, the matrix is not located in the recycle path. As such, due to the differences in structural arrangement, airflow passage, mass flow rate, and the thermophysical properties of the porous medium, a direct comparison between the results of the two studies is not feasible. The interpretation of the outcomes must therefore take these differences into account.

At a return ratio of G = 1 and mass flow rates above 0.015 kg/s, the thermo-hydraulic efficiency of Types 3, 4, and 5 declines with increasing flow rate due to intensified pressure losses caused by internal obstructions.

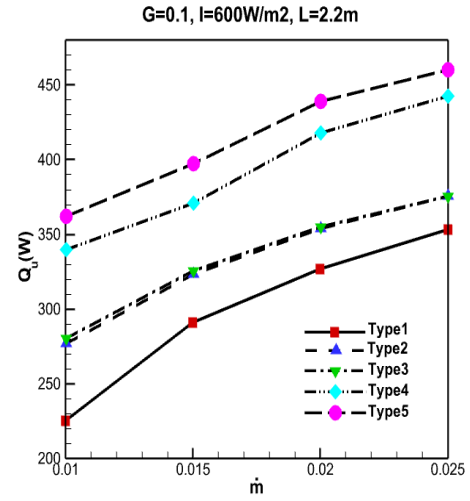

(a) G=0.1

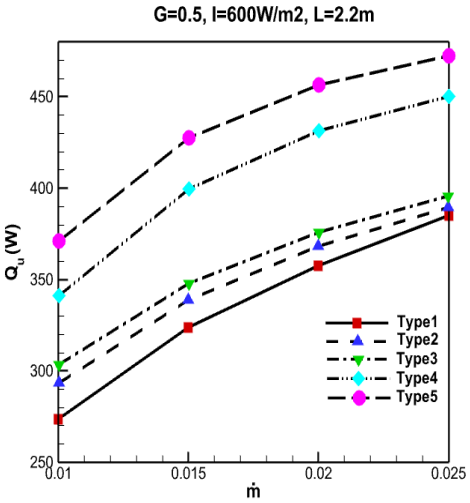

(b) G=0.5

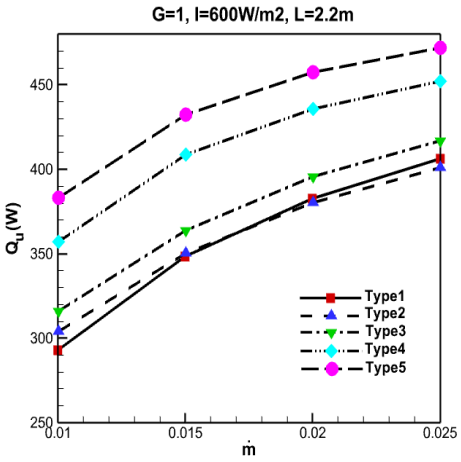

(c) G=1

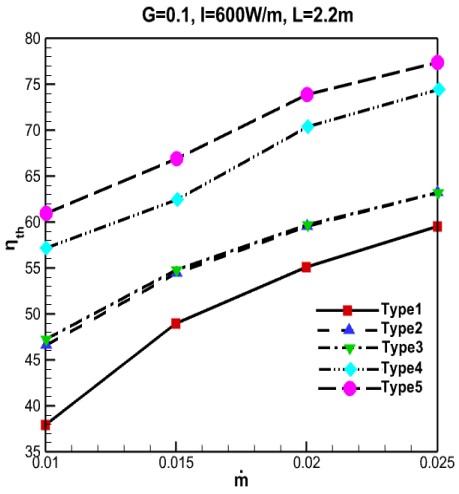

(d) G=0.1

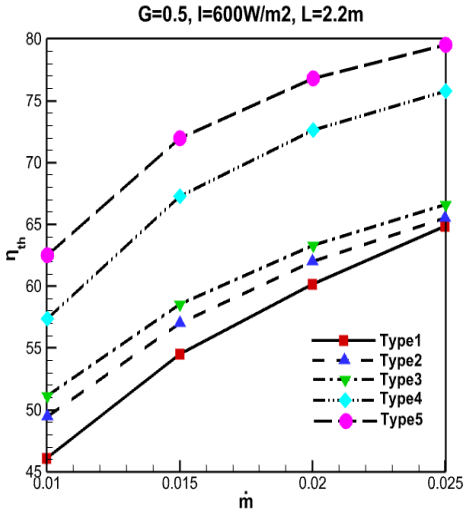

(e) G=0.5

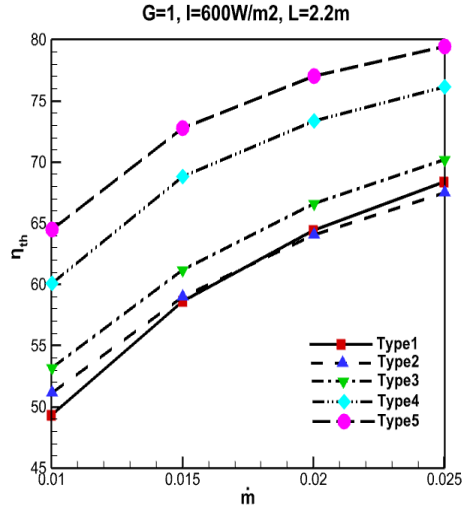

(f) G=1

Fig. 5. Variation of useful heat gain and thermal efficiency for I = 600 W/m2 against the air mass flow rate: (a) Q_u for G=0.1, (b) Q_u for G=0.5, (c) Q_u for G=1, (d) η_{th} for G=0.1, (e) η_{th} for G=0.5, (f) η_{th} for G=1.

Table 6. Comparison of useful heat gain (W), thermal efficiency, and thermo-hydraulic efficiency at two solar irradiance levels (600 and 800 W/m²).

	G	I=600 ṁ=0.01			I=800 ṁ=0.01			I=600 ṁ=0.025			I=800 ṁ=0.025		
		Q_u	η_{th}	η_{thy}	Q_u	η_{th}	η_{thy}	Q_u	η_{th}	η_{thy}	Q_u	η_{th}	η_{thy}
Type 1	0.1	225.1427	37.9	37.9	288.0141	36.37	36.37	353.5471	59.52	59.52	464.1404	58.6	58.6
	0.5	273.8338	46.1	46.1	353.8768	44.68	44.68	385.188	64.85	64.84	508.85	64.25	64.24
	0.9	289.6858	48.77	48.77	375.7278	47.44	47.44	403.2645	67.89	67.87	534.3097	67.46	67.45
Type 2	0.1	276.9742	46.63	46.26	360.3644	45.5	45.21	375.4058	63.2	59.56	497.1342	62.77	59.97
	0.5	293.6084	49.43	48.6	383.6109	48.44	47.79	389.2402	65.53	57.45	516.6533	65.23	59.03
	0.9	302.1975	50.88	49.34	395.5882	49.95	48.74	399.2545	67.21	52.32	530.8476	67.03	55.55
Type 3	0.1	280.6172	47.24	46.69	364.8405	46.07	45.63	375.6039	63.23	57.88	495.9095	62.61	58.49
	0.5	303.6837	51.13	49.9	395.8704	49.98	49.02	395.7276	66.62	54.76	523.8645	66.14	57.02
	0.9	314.1298	52.88	50.61	410.1808	51.79	50	414.2560	69.74	47.83	550.1704	69.47	52.52
Type 4	0.1	339.4959	57.15	56.86	444.0787	56.07	55.84	442.3099	74.46	70.33	589.7734	74.47	71.3
	0.5	341.0243	57.41	56.63	446.4124	56.37	55.76	450.0787	75.77	64.92	601.288	75.92	67.66
	0.9	353.9592	59.59	57.88	465.0218	58.71	57.39	452.1438	76.12	53.11	604.4838	76.32	58.78
Type 5	0.1	362.2282	60.98	60.68	473.0009	59.72	59.49	459.8988	77.42	73.23	613.3432	77.44	74.25
	0.5	371.2424	62.5	61.76	484.7116	61.2	60.63	472.2307	79.5	69.12	631.4539	79.73	71.82
	0.9	381.1574	64.17	62.69	499.6463	63.09	61.95	472.3228	79.52	58.72	631.9588	79.79	63.95

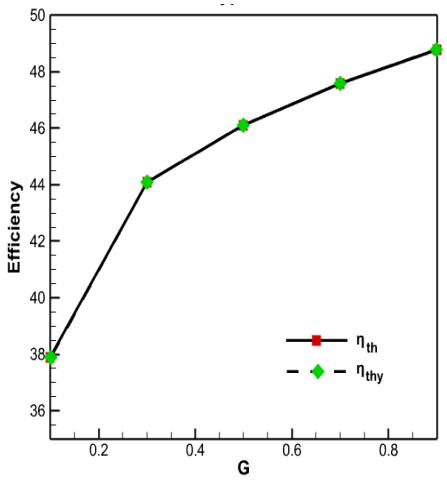

(a) Type 1

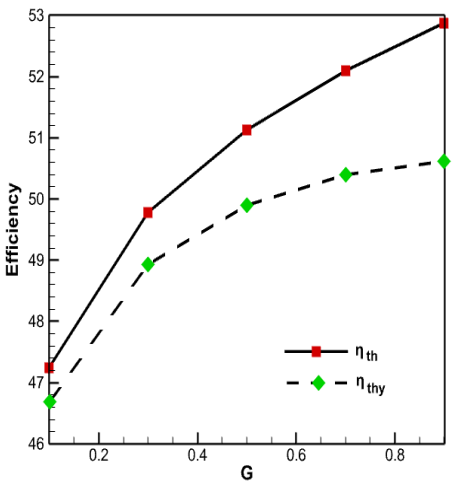

(c) Type 3

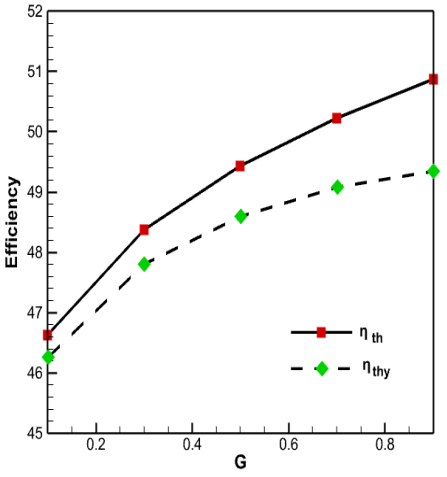

(b) Type 2

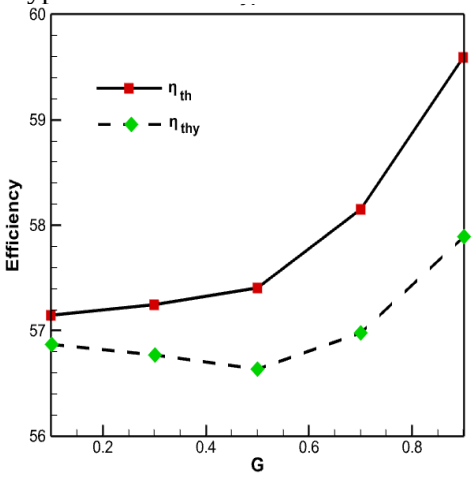

(d) Type 4

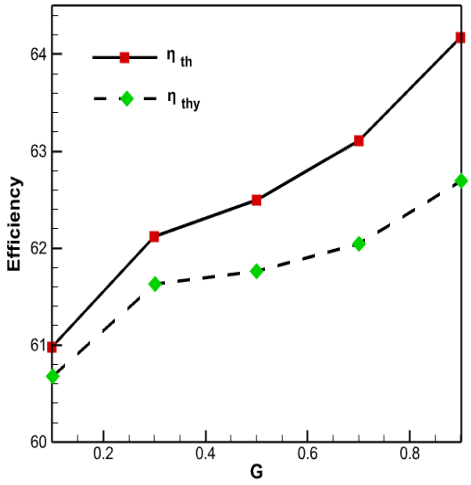

(e) Type 5

Fig. 6. The changes in thermo-hydraulic and thermal efficiencies as a function of the reflux ratio, considering 0.01 kg/s mass flow rate: (a) Type1, (b) Type2, (c) Type3, (d) Type4, (e) Type5.

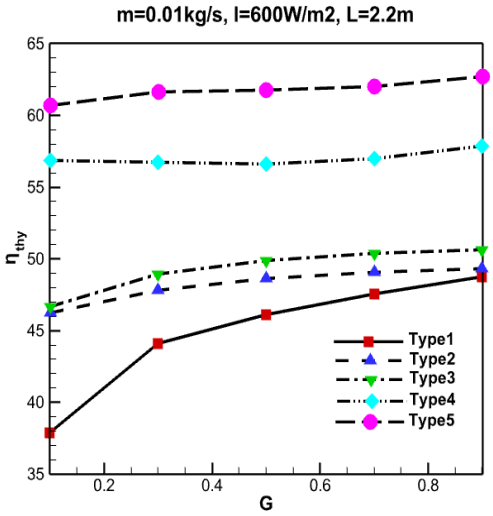

Fig. 7. Variation of thermo-hydraulic efficiency against the reflux ratio.

These structural variations also manifest in the form of differing pressure losses, which in turn influence the thermo-hydraulic performance of each configuration. This effect becomes particularly evident when examining how efficiency responds to changes in mass flow rate, as discussed below.

For Type 3, which contains a porous matrix beneath the absorber plate, the decline is attributed to the high flow resistance induced by the matrix [19].

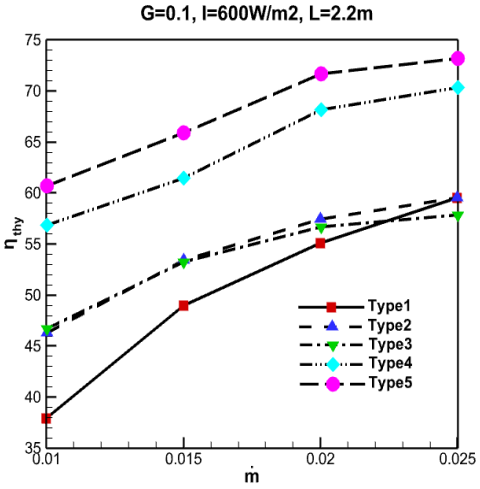

(a) G=0.1

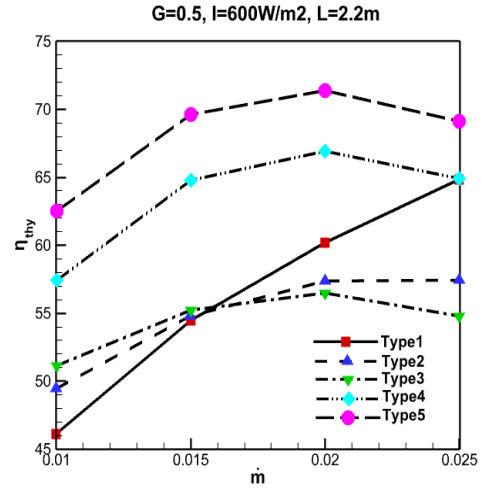

(b) G=0.5

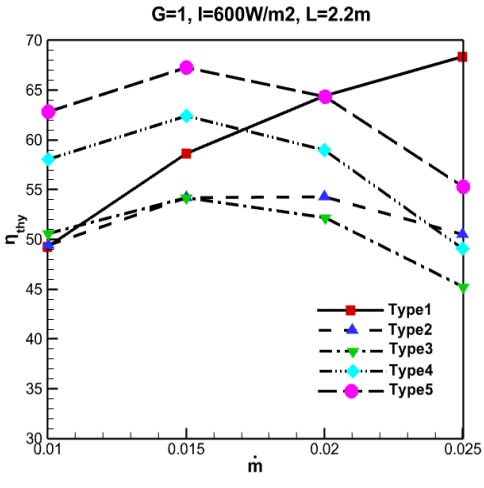

(c) G=1

Fig. 8. Variation of thermo-hydraulic efficiency against the air mass flow rate: (a) G=0.1, (b) G=0.5, (c) G=1.

In Type 5, which includes only baffles, the increased frictional losses at high flow rates reduce performance [5]. Type 4, which combines both features, suffers from compounded losses. In contrast, the thermo-hydraulic efficiency of Type 1 air heater, which lacks internal obstructions, improves with increasing mass flow rate, and at G = 1 and m > 0.02 kg/s, it outperforms the other types due to its minimal pressure drop.

The observed trends in thermo-hydraulic efficiency in Fig. 8 can be better understood by examining the Reynolds number ranges where Types 3 and 5 transition from laminar to turbulent flow, along with the corresponding behavior of the Nusselt number (Nu) and friction factor (f).

For Type 3, which features a porous matrix in the lower channel, the main flow remains laminar up to a Reynolds number of approximately 1166 and transitions to turbulent flow near 2505. Within this transitional range, Nu increases from about 5.6 to 13, while the friction factor decreases from 0.0122 to 0.0072. Although turbulent flow enhances heat transfer, the high hydraulic resistance caused by the matrix limits the overall thermo-hydraulic performance, especially at higher return ratios.

In contrast, Type 5, with fins and baffles in the upper main channel, experiences turbulent flow even at lower Reynolds numbers around 900. As the mass flow rate increases, the Reynolds number exceeds 3000, Nu rises from 108.7 to 312.2, and the friction factor drops from 0.0474 to 0.0079. This combination of enhanced heat transfer and moderate pressure drop results in consistently higher thermo-hydraulic efficiency compared to Type 3. At a return ratio of 0.5, the recovery channel transitions from laminar to turbulent flow near Re = 675, causing an initial increase in heat transfer up to around 0.02 kg/s mass flow rate, beyond which increasing pressure losses reduce overall efficiency.

At a low return ratio of 0.1, thermo-hydraulic efficiency rises steadily with increasing mass flow rate due to relatively low-pressure losses and earlier transition to turbulence, particularly in Type 5. However, at a high return ratio of 1, Types 3, 4, and 5 show a decline in efficiency beyond approximately 0.015 kg/s, mainly because of increased frictional losses that offset heat transfer gains. Under these conditions, Type 1 — lacking internal enhancements — benefits from lower pressure drops and surpasses other configurations in efficiency at mass flow rates above 0.02 kg/s.

Overall, the superior performance of Type 5 stems from its early transition to turbulent flow and balanced increase in heat transfer relative to pressure drop, while the delayed turbulence onset and high hydraulic resistance of the porous matrix constrain Type 3's efficiency, especially at higher return ratios and flow rates.

These findings highlight the critical role of flow regime transition and hydraulic resistance in determining the overall thermo-hydraulic efficiency of solar air heater configurations. In particular, configurations such as Type 5, which incorporates a fin and baffle arrangement that promotes early turbulence onset while maintaining a controlled pressure drop, exhibit superior performance. This emphasizes the importance of carefully optimizing internal enhancements to strike an effective balance between heat transfer improvement and pressure loss, as supported by previous studies[3,5,9].

- Analysis of why fins and baffles outperform the matrix configuration

A closer examination of the simulation results demonstrates that the superior thermal and thermo-hydraulic performance of the solar air heater with fins and baffles (Type 5) compared to those using porous matrices (Types 2–4) stems from two primary mechanisms: enhanced turbulence and increased effective heat transfer area.

The baffles promote flow separation and reattachment, intensifying turbulence and facilitating strong mixing. Simultaneously, the longitudinal fins provide a significant increase in heat transfer surface area while maintaining excellent thermal contact with the absorber plate. Together, these effects result in a thinner thermal boundary layer and substantially elevated convective heat transfer, as evidenced by an increase in the Nusselt number (Nu) [1,4].

Qualitatively, the configurations can be ranked in terms of Nu and overall performance as: Type 5 > Type 4 > Type 3 > Type 2 > Type 1.
While porous matrices also increase surface area and introduce some level of turbulence, they come at the cost of significant flow resistance [12,23]. For example, Type 4, where the matrix is placed in the recycle path, suffers from considerable pressure drop and higher fan power requirements. In Type 3, the matrix is located below the absorber plate, which facilitates fluid mixing but causes delayed heat absorption due to the indirect thermal path. Additionally, all matrix configurations tend to generate higher friction factors, reducing the overall thermo-hydraulic efficiency.
In contrast, the fin–baffle configuration in Type 5 strikes an optimal balance by maximizing convective enhancement and surface area while maintaining moderate pressure losses [1,4,5]. This design leads to the highest values of both thermal efficiency and thermo-hydraulic efficiency across all operating conditions.

5. Conclusions

Solar energy, as a clean and renewable resource, plays a critical role in addressing global energy challenges. Solar air heaters, in particular, offer an efficient means of harnessing this energy, contributing to sustainable heating solutions while reducing reliance on conventional fossil fuels.
This study comprehensively investigates the efficiency of the solar air heater incorporating an internal recycle across five different configurations, focusing on thermal and thermo-hydraulic efficiency analysis. These configurations include: a conventional design, two systems where a porous matrix is placed either beneath or above the absorber plate, a setup with fins and baffles on the absorber plate, and finally, a combination featuring both fins and baffles on the absorber plate along with a porous matrix in the recycle path.
The study also examined the effects of several performance parameters, including variations in reflux ratio, air mass flow rate, and solar irradiance on the collector surface, on the thermo-hydraulic and thermal efficiencies of the DPSAH. To ensure the reliability of the findings, the results of this study were validated using the data from the research of Ahmadkhani *et al.* [2]. The comparison demonstrated a high degree of accuracy, as the discrepancy in the computed thermal efficiency remained below 2%, confirming the robustness of the proposed approach.
The key findings of this research are as follows:

- An increase in the reflux ratio (G) improves both useful heat gain and thermal efficiency across the various solar air heaters.
- The solar air heater with fins and baffles exhibits significantly higher useful heat gain, thermal and thermo-hydraulic performances compared to other configurations. At a mass flow rate of 0.015 kg/s and a reflux ratio of 0.5, where its thermal efficiency is approximately 13.5% greater than that of the configuration with the matrix beneath the absorber plate. Thus, under similar conditions, it is recommended to use fins and baffles to enhance these efficiencies.
- At mass flow rates of 0.01 kg/s and 0.015 kg/s, incorporating a matrix in the main air passage enhances useful heat gain and thermal efficiency. However, at a mass flow rate of 0.025 kg/s and a reflux ratio below 0.7, the improvement trend continues.
- The presence of the matrix intensifies airflow disturbance and promotes more effective heat exchange, thereby increasing the air temperature in the corresponding channel. The use of a matrix leads to a substantial pressure drop, increasing the energy demand on the fan, which must be taken into account.
- As the reflux ratio increases, placing the matrix beneath the absorber plate results in higher thermal efficiency and useful heat gain. At a reflux ratio of 0.1, there is minimal difference in useful heat gain and thermal efficiency between configurations with a matrix above and below the absorber plate, indicating a limited impact of matrix positioning at lower reflux ratios. At reflux ratios of 0.5 and 1, the configuration with the matrix beneath the absorber plate yields higher useful heat and thermal efficiency compared to the one with the matrix above the absorber plate. However, if pressure drop and fan energy are significant considerations, it is

better to place the matrix above the absorber plate at higher mass flow rates, as this arrangement results in lower pressure drop.

- As solar radiation intensity increases, the useful heat absorbed rises; however, this does not guarantee an increase in thermal efficiency, as the relative increase in useful heat (Qu) and solar radiation (I) determines the overall efficiency.
- The thermal efficiency of the configuration without a matrix is approximately equal to its thermo-hydraulic efficiency due to low pressure drops. In contrast, in other configurations with matrices or fins, thermo-hydraulic efficiency is generally lower.
- If pressure drop and fan power in air heater design are critical, thermo-hydraulic efficiency should be prioritized. For return ratios from G=0.1 to G=0.5 and across all examined mass flow rates, the use of fins and baffles to enhance efficiency in air heater structures is recommended. At a return ratio of G=1 and m>0.018 kg/s, the thermo-hydraulic performance of a conventional internal recycle solar air heater is greater than other types due to the absence of matrices, fins, or baffles, resulting in a lower pressure drop.
- Solar air heaters equipped with fins, baffles, and a porous matrix under recycle conditions show improved thermal and thermo-hydraulic efficiencies, particularly at low mass flow rates, compared to conventional solar air heaters with internal recycling. However, when comparing the thermal and thermo-hydraulic efficiencies of this type of solar air heater to one that uses only fins and baffles on the absorber plate, it becomes clear that adding the matrix does not improve efficiency and may even reduce overall performance.

This study is novel in presenting a first-of-its-kind comparative performance analysis of solar air heater designs integrating porous matrix and enhanced convective elements (fins and baffles) under identical operational conditions. The results offer valuable guidelines for the optimal design of hybrid systems in solar applications.

Acknowledgment

The authors would like to express their deep gratitude to the Energy Research Institute of the University of Kashan for their generous support and resources provided during this research.

References

[1] A. Ghiami and S. Ghiami, “Comparative study based on energy and exergy analyses of a baffled solar air heater with latent storage collector,” *Appl. Therm. Eng.*, Vol. 133, pp. 797–808, (2018).

[2] A. Ahmadkhani, G. Sadeghi, and H. Safarzadeh, “An in-depth evaluation of matrix, external upstream and downstream recycles on a double pass flat plate solar air heater efficacy,” *Therm. Sci. Eng. Prog.*, Vol. 21, p. 100789, (2021).

[3] S. Singh and P. Dhiman, “Analytical and experimental investigations of packed bed solar air heaters under the collective effect of recycle ratio and fractional mass flow rate,” *J. Energy Storage*, Vol. 16, pp. 167–186, (2018).

[4] K. Mohammadi and M. Sabzpooshani, “Appraising the performance of a baffled solar air heater with external recycle,” *Energy Convers. Manag.*, Vol. 88, pp. 239–250, (2014).

[5] K. Mohammadi and M. Sabzpooshani, “Comprehensive performance evaluation and parametric studies of single pass solar air heater with fins and baffles attached over the absorber plate,” *Energy*, Vol. 57, pp. 741–750, (2013).

[6] F. Chabane, N. Moummi, and S. Benramache, “Experimental study of heat transfer and thermal performance with longitudinal fins of solar air heater,” *J. Adv. Res.*, Vol. 5, No. 2, pp. 183–192, (2014).

[7] R. Karwa, “Thermo-hydraulic performance of solar air heater with finned absorber plate forming multiple rectangular air flow passages in parallel under laminar flow conditions,” *Appl. Therm. Eng.*, Vol. 221, p. 119673, (2023).

[8] A. Ahmad, J. S. Saini, and H. K. Varma, “Effect of geometrical and thermophysical characteristics of bed materials on the

enhancement of thermal performance of packed bed solar air heaters," *Energy Convers. Manag.*, Vol. 36, No. 12, pp. 1185–1195, (1995).

[9] A. Ahmad, J. S. Saini, and H. K. Varma, "Thermohydraulic performance of packed-bed solar air heaters," *Energy Convers. Manag.*, Vol. 37, No. 2, pp. 205–214, (1996).

[10] A. A. El-Sebaii, S. Aboul-Enein, M. R. I. Ramadan, and E. El-Bialy, "Year round performance of double pass solar air heater with packed bed," *Energy Convers. Manag.*, Vol. 48, No. 3, pp. 990–1003, (2007).

[11] P. Velmurugan and R. Kalaivanan, "Energy and Exergy Analysis of Solar Air Heaters with Varied Geometries," *Arab. J. Sci. Eng.*, Vol. 40, No. 4, pp. 1173–1186, (2015).

[12] P. Dhiman and S. Singh, "Recyclic double pass packed bed solar air heaters," *Int. J. Therm. Sci.*, Vol. 87, pp. 215–227, (2015).

[13] H. M. Yeh and C. D. Ho, "Solar air heaters with external recycle," *Appl. Therm. Eng.*, Vol. 29, No. 8–9, pp. 1694–1701, (2009).

[14] A. P. Omojaro and L. B. Y. Aldabbagh, "Experimental performance of single and double pass solar air heater with fins and steel wire mesh as absorber," *Appl. Energy*, Vol. 87, No. 12, pp. 3759–3765, (2010).

[15] A. M. Ebrahim Momin, J. S. Saini, and S. C. Solanki, "Heat transfer and friction in solar air heater duct with V-shaped rib roughness on absorber plate," *Int. J. Heat Mass Transf.*, Vol. 45, No. 16, pp. 3383–3396, (2002).

[16] Varun, R. P. Saini, and S. K. Singal, "A review on roughness geometry used in solar air heaters," *Sol. Energy*, Vol. 81, No. 11, pp. 1340–1350, (2007).

[17] V. S. Hans, R. P. Saini, and J. S. Saini, "Heat transfer and friction factor correlations for a solar air heater duct roughened artificially with multiple v-ribs," *Sol. Energy*, Vol. 84, No. 6, pp. 898–911, (2010).

[18] R. K. Ravi and R. P. Saini, "Nusselt number and friction factor correlations for forced convective type counter flow solar air heater having discrete multi V shaped and staggered rib roughness on both sides of the absorber plate," *Appl. Therm. Eng.*, Vol. 129, pp. 735–746, (2018).

[19] S. Singh, "Utilising fractional porous interface for high thermal performance of serpentine wavy channel solar air heater," *Appl. Therm. Eng.*, Vol. 205, p. 118044, (2022).

[20] F. P. Incropera, D. P. DeWitt, T. L. Bergman, and A. S. Lavine, Fundamentals of Heat and Mass Transfer, 7th ed. Wiley, 2011.

[21] Y. A. Çengel and A. J. Ghajar, Heat and Mass Transfer: Fundamentals and Applications, 5th ed. McGraw-Hill, 2015.

[22] K. Sopian, M. A. Alghoul, E. M. Alfegi, M. Y. Sulaiman, and E. A. Musa, "Evaluation of thermal efficiency of double-pass solar collector with porous–nonporous media," *Renew. Energy*, Vol. 34, No. 3, pp. 640–645, (2009).

[23] N. S. Thakur, J. S. Saini, and S. C. Solanki, "Heat transfer and friction factor correlations for packed bed solar air heater for a low porosity system," *Sol. Energy*, Vol. 74, No. 4, pp. 319–329, (2003).

[24] P. Dhiman, N. S. Thakur, and S. R. Chauhan, "Thermal and thermohydraulic performance of counter and parallel flow packed bed solar air heaters," *Renew. Energy*, Vol. 46, pp. 259–268, (2012).